RSC Advances

PAPER

View Article Online
View Journal | View Issue

Cite this: *RSC Adv.*, 2026, **16**, 25927

Thermodynamic description of $Eu(NO_3)_3$-$NaNO_3$-H_2O and $Eu(NO_3)_3$-$Mg(NO_3)_2$-H_2O systems. Solubility experiments and full dissociation Pitzer models

F. Häusler, *[a] P. F. dos Santos, [a] A. Lassin, *[b] X. Gaona, [a] K. Garbev, [c] S. Touzelet,[b] Y. Cartigny,[d] M. Altmaier[a] and B. Madé[e]

Received 2nd December 2025
Accepted 11th February 2026

DOI: 10.1039/d5ra09321j

rsc.li/rsc-advances

Solubility studies in the systems $Eu(NO_3)_3$-$NaNO_3$-H_2O and $Eu(NO_3)_3$-$Mg(NO_3)_2$-H_2O were conducted at $T = (22 \pm 2)$ °C including solid phase identification by X-ray powder diffraction and Schreinemakers' method. Iso-water activity data of both systems at 25 °C were determined by iso-water activity (IWA) and dynamic vapor sorption (DVS) experiments. These experimental results were collectively used to verify and complement existing sets of Pitzer interaction parameters for the ternary systems. The resulting thermodynamic models assume the full dissociation of all involved salts. The geochemical code PhreeSCALE was used together with the parameter estimation software PEST to determine new ternary interaction parameters $\Psi_{Eu^{3+},Na^+,NO_3^-}$, and $\Psi_{Eu^{3+},Mg^{2+},NO_3^-}$. In combination with our previous work on Na_2SO_4 and $MgSO_4$ solutions [F. dos Santos *et al.*, 2024, *Dalton Trans.*, 53, 6289–6299], the updated model allows an accurate description of Eu(III) solubility in complex nitrate–sulphate systems of relevance for radioactive waste disposal.

Introduction

The rare-earth element europium is well known for its luminescence, which has led to versatile applications in light and display technology, security inks, biomedical analysis, and agriculture.[1,2] As part of the lanthanide series, Eu(III) is, due to its similar solution chemistry and aqueous speciation, also considered an analogue for trivalent actinides such as Am(III) and Pu(III) and is therefore of importance for research in the field of radioactive waste disposal, where both actinides play a predominant role.[2,3]

Considerable quantities of nitrate are part of the disposal inventory in several streams of long-lived intermediate-level and long-lived low-level radioactive waste.[4,5] In particular, reprocessing techniques using nitric acid to recover radionuclides result in significant inventories of nitrate-rich waste.[6–9] Nitrate is known to be an oxidizing agent and therefore able to influence the redox chemistry within a nuclear waste repository.[10,11] A comprehensive understanding of the solution chemistry of nitrate systems is also required to predict interactions with (geo-)technical barriers and the impact on radionuclide retention.

Aqueous nitrate systems are known for high ionic strength due to the comparatively high solubility of nitrate salts.[12–16] To properly describe the chemical behaviour of such systems, it is thus important to collect sufficient experimental data over a wide concentration range and use models able to reproduce solution properties and solubility behaviour at high ionic strength. The Pitzer model[17,18] fulfils this requirement and is therefore used in the present work. Following the full dissociation approach and taking advantage of specific interaction parameters previously published for the binary systems, sets of Pitzer parameters are proposed to properly describe the two ternary systems $Eu(NO_3)_3$-$NaNO_3$-H_2O and $Eu(NO_3)_3$-$Mg(NO_3)_2$-H_2O. New investigations on solubility in diluted to concentrated aqueous solutions (up to 5.3 mol $NaNO_3$ per kg H_2O and 4.3 mol $Mg(NO_3)_2$ per kg H_2O) and iso-water activity experiments were conducted as the data basis for the parameter estimation process. Future work will focus separately upon the alternative partial dissociation approach, which considers the formation of aqueous metal–nitrate complexes and includes SIT (specific ion interaction theory) and Pitzer models as well as complementary spectroscopic data on Eu(III)-NO_3^- speciation.

Experimental

Chemicals

Solutions were prepared with ultrapure water, purified with a Milli-Q Academic apparatus (Merck Millipore, 18.2 MΩ cm, 22

[a]*Institute for Nuclear Waste Disposal, Karlsruhe Institute of Technology, Karlsruhe, Germany. E-mail: felix.haeusler@kit.edu; a.lassin@brgm.fr*
[b]*BRGM, F-45060 Orléans, France*
[c]*Institute for Technical Chemistry, Karlsruhe Institute of Technology, Karlsruhe, Germany*
[d]*SMS, Univ. Rouen Normandie, F-76821 Mont Saint Aignan, France*
[e]*Scientific and Technical Division, Andra, Châtenay-Malabry, France*

± 2 °C, pore size: 0.22 μm). Anhydrous sodium nitrate ($NaNO_3$, p.a., 99 wt%), magnesium nitrate hexahydrate ($Mg(NO_3)_2 \cdot 6H_2O$, p.a., 99 wt%), europium(III) nitrate hexahydrate ($Eu(NO_3)_3 \cdot 6H_2O$, p.a., 99.9 wt%) and europium(III) sulphate octahydrate ($Eu_2(SO_4)_3 \cdot 8H_2O$, p.a., 99.9 wt%) were purchased from Thermo Fisher Scientific. Anhydrous sodium sulphate (Na_2SO_4, p.a., 99 wt%) was purchased from Merck.

Solubility experiments

Solubility studies were performed with different series of independent batch experiments from undersaturation conditions. Nine and twelve samples for the systems $Eu(NO_3)_3$-$NaNO_3$-H_2O and $Eu(NO_3)_3$-$Mg(NO_3)_2$-H_2O were equilibrated at $T = (22 \pm 2)$ °C over concentration ranges of 0.0–5.3 mol $NaNO_3$ per kg H_2O and 0.0–4.3 mol $Mg(NO_3)_2$ per kg H_2O, respectively. The pH values of these samples were determined with an Orion 8103SC pH glass electrode (Thermo Scientific) after calibration with three commercial calibration buffer solutions of pH = 1, 4, and 7. An additional set of six samples was prepared for the quaternary system $Eu_2(SO_4)_3$-$Eu(NO_3)_3$-Na_2SO_4-$NaNO_3$-H_2O with 1.3–4.5 mol $NaNO_3$ per kg H_2O and 0.8–1.6 mol Na_2SO_4 per kg H_2O. Experiments in pure nitrate systems were conducted from

Table 1 Solubility data and solid phase characterization of this work for the systems $Eu(NO_3)_3$-H_2O, $Eu(NO_3)_3$-$NaNO_3$-H_2O and $Eu(NO_3)_3$-$Mg(NO_3)_2$-H_2O at (22 ± 2) °C and pH ≤ 3.8

$Eu(NO_3)_3$-H_2O

m($Eu(NO_3)_3$) in mol per kg H_2O	XRPD sample	Solid phase[a]	Rietveld refinement results in wt% (e.s.d.)		
			$Eu(NO_3)_3 \cdot 6H_2O$	$Eu(NO_3)_3(H_2O)_4(H_2O)$	$NaNO_3$
4.22 ± 0.34	A	$Eu(NO_3)_3 \cdot 6H_2O$	70(1)	30(1)	—

$Eu(NO_3)_3$-$NaNO_3$-H_2O

m($NaNO_3$) in mol per kg H_2O	m($Eu(NO_3)_3$) in mol per kg H_2O	XRPD sample	Solid phase[a]			
0.68 ± 0.12	4.31 ± 0.35	B	$Eu(NO_3)_3 \cdot 6H_2O$	90(1)	10(1)	—
1.24 ± 0.19	4.34 ± 0.27	C	$Eu(NO_3)_3 \cdot 6H_2O$	81(4)	19(4)	—
2.37 ± 0.24	4.40 ± 0.39					
2.75 ± 0.21	4.18 ± 0.18	D	$Eu(NO_3)_3 \cdot 6H_2O$ + $NaNO_3$	71(2)	12(1)	17(2)
3.73 ± 0.21	3.27 ± 0.11					
3.81 ± 0.16	3.16 ± 0.19	E	$NaNO_3$	—	—	100
5.26 ± 0.24	2.29 ± 0.14					
5.00 ± 0.22	2.30 ± 0.14	F	$NaNO_3$	—	—	100

$Eu(NO_3)_3$-$Mg(NO_3)_2$-H_2O

m($Mg(NO_3)_2$) in mol per kg H_2O	m($Eu(NO_3)_3$) in mol per kg H_2O	XRPD sample	Solid phase[a,b]	Rietveld refinement results in wt% (e.s.d.)		
				$Eu(NO_3)_3 \cdot 6H_2O$	$Eu(NO_3)_3(H_2O)_4(H_2O)$	$Mg(NO_3)_2 \cdot 6H_2O$
0.31 ± 0.03	3.80 ± 0.11	G	$Eu(NO_3)_3 \cdot 6H_2O$	97(1)	3(1)	—
1.09 ± 0.08	3.38 ± 0.15	H	$Eu(NO_3)_3 \cdot 6H_2O$	97(1)	3(1)	—
1.75 ± 0.13	2.96 ± 0.12	I	$Eu(NO_3)_3 \cdot 6H_2O$	80(3)	20(3)	—
2.96 ± 0.24	2.33 ± 0.08	J	$Eu(NO_3)_3 \cdot 6H_2O$	59(3)	41(3)	—

$Eu(NO_3)_3$-$Mg(NO_3)_2$-H_2O

m($Mg(NO_3)_2$) in mol per kg H_2O	m($Eu(NO_3)_3$) in mol per kg H_2O	XRPD sample	Solid phase[a,b]
3.63 ± 0.17	1.90 ± 0.06	K	$2Eu(NO_3)_3 \cdot 3Mg(NO_3)_2 \cdot 24H_2O$ + $Mg(NO_3)_2 \cdot 6H_2O$
3.18 ± 0.01	1.97 ± 0.02	L	$Eu(NO_3)_3 \cdot 6H_2O$
3.40 ± 0.01	1.91 ± 0.02	M	$Eu(NO_3)_3 \cdot 6H_2O$
3.38 ± 0.03	1.88 ± 0.01	N	$Eu(NO_3)_3 \cdot 6H_2O$ + $Mg(NO_3)_2 \cdot 6H_2O$
4.31 ± 0.02	0.51 ± 0.01	O	$Mg(NO_3)_2 \cdot 6H_2O$
3.96 ± 0.03	1.11 ± 0.01	P	$Mg(NO_3)_2 \cdot 6H_2O$
3.50 ± 0.03	1.65 ± 0.01	Q	$Mg(NO_3)_2 \cdot 6H_2O$
3.38 ± 0.03	1.86 ± 0.01	R	$Eu(NO_3)_3 \cdot 6H_2O$ + $Mg(NO_3)_2 \cdot 6H_2O$

[a] Identification of solid phases: XRPD. [b] Schreinemakers' method.

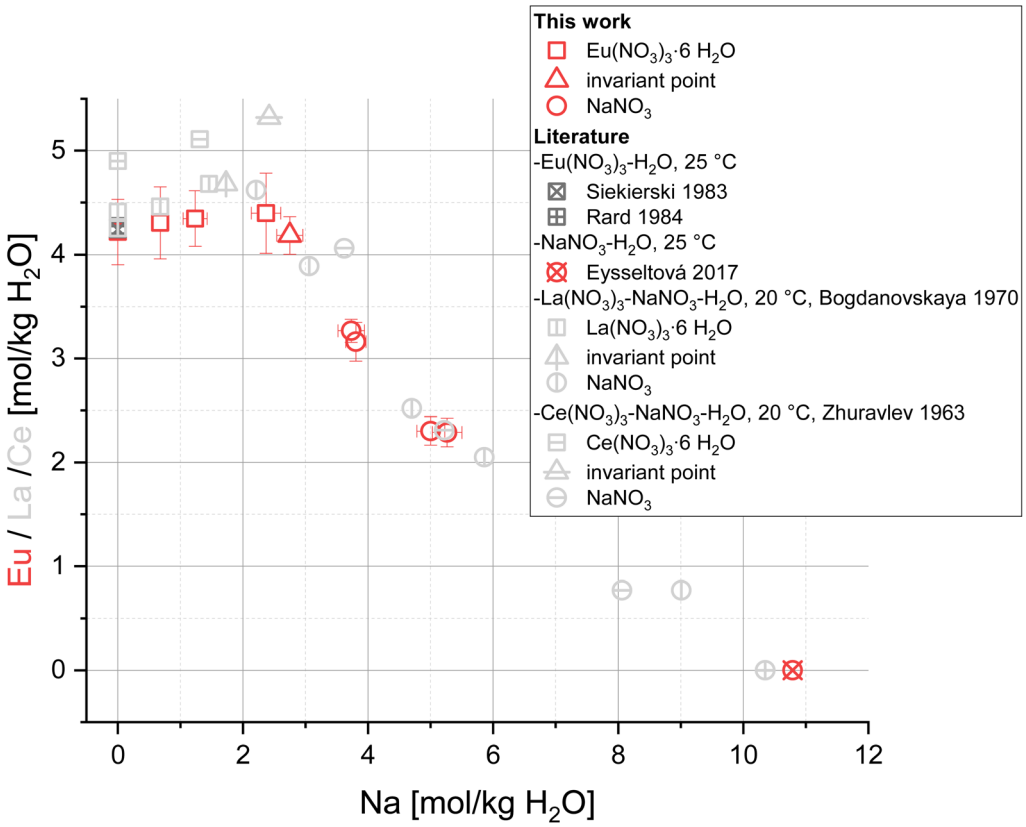

Fig. 1 Solubility data for the system $Eu(NO_3)_3$-$NaNO_3$-H_2O (red) at $T = (22 \pm 2)$ °C (complemented by literature data for solubilities in the binary subsystems at 25 °C [12–14]) compared to solubility data of the systems $La(NO_3)_3$-$NaNO_3$-H_2O and $Ce(NO_3)_3$-$NaNO_3$-H_2O (light grey).[53,54]

undersaturation conditions with $Eu(NO_3)_3 \cdot 6H_2O$, whereas $Eu_2(SO_4)_3 \cdot 8H_2O$ was used for solubility in mixed nitrate–sulphate solutions. All samples were subjected to constant agitation until thermodynamic equilibrium was reached, which was assumed after repeated measurements showing constant total Eu(III) concentration. Sampling was performed several times over a period of up to 21 months. Solid and liquid phases were separated by ultrafiltration (10 kDa ≈ 2 nm, Pall Life Science), followed by the dilution of solutions with HNO_3 (2%). A dilution factor between 10 000 and 50 000 was applied for analysis due to the high salt concentrations. Eu, Na, Mg, and S concentrations were then measured *via* ICP-OES (Inductively Coupled Plasma Optical Emission Spectroscopy, PerkinElmer Optima 8300 DV). The uncertainty of ICP-OES measurements is below 5%. Uncertainties for solubility data depicted in the related figures are calculated as standard deviations of the average of single measurements for each sample (>15 measurements per sample).

Iso-water activity (IWA) and dynamic vapor sorption (DVS) experiments

To add constraints to specific ion interaction optimization, experiments were carried out to measure the chemical composition of synthetic brines at equilibrium with fixed relative humidities at 25 °C. The principle is the following: an aqueous mixture of known composition and mass is placed in an environment of fixed relative humidity and temperature. Its mass is monitored continuously over several hours to days until it stabilizes, which is representative of thermodynamic equilibrium. The mass variation is due to water gain or loss, and its final value therefore indicates the chemical composition of the brine at equilibrium with the stipulated relative humidity, equivalent of the water activity. This iso-water activity (IWA) technique is similar to isopiestic measurements,[20] with the difference that water activity is imposed by means of controlled relative humidity.[9,21,22]

Two different apparatuses were used. The first one is a climatic chamber C-20/350 (CTS GmbH), whose internal volume is 350 L. Temperature and relative humidity can be varied in the ranges −20–180 °C, and 10–98%, respectively. The uncertainty of the measured temperature and relative humidity is 0.03 °C and 1.5%, respectively. A beaker of 100 mL was placed in the climatic chamber on a balance (Combics 3, Sartorius Weighing Technology GmbH, precision of 0.01 g) and the brine was continuously stirred with a paddle. The initial mass of the salt solution was *ca.* 50 g. At the end of the experiment for a given relative humidity, the weight was measured without the paddle to avoid Archimedes' buoyancy. Then, a new value of the relative humidity was set for a new experiment. The chamber needs to be opened for 1–2 minutes to adjust the paddle. The following stabilization of temperature and relative humidity takes about one hour. The frequency of measurements was once

per day to ensure sufficient equilibration time and minimization of the error in weight measurement.

The second apparatus is a dynamic vapor sorption (DVS) device DVS One (Surface Measurement Systems, Wembley, UK). In this apparatus, the temperature (±0.5 °C) and the relative humidity (±0.5%) are regulated, while the mass variation is recorded by a microbalance (±0.1 μg). Samples were submitted to the successive desorption–sorption cycles (80–50% relative humidity with a step size of 10% RH). The fixed criterion for the step change was a mass variation of the sample lower than 0.0005% per minute in the limit of 2000 min per step. The DVS device is composed of a thermostatic chamber with two closed vessels; each contains a suspended cup connected to a balance. A drop (*i.e.* less than 0.1 g) of the brine to study was placed in one cup, while the second cup remained empty as reference. Like in the climatic chamber, the relative humidity is set in the air that flows independently through the two vessels. Here again, the relative mass variation indicates the variation of the chemical composition of the brine due to water evaporation or condensation. The mass is continuously measured without the need to open the chamber. Because of the much smaller masses of brine used with the DVS device, experiments reach equilibrium faster than in the climatic chamber.

For both methods the chambers rely on the mixture of humid and dry air to set the targeted relative humidity, which is a method not expected to impact the equilibria.

X-ray powder diffraction (XRPD)

Solid phases were identified by X-ray powder diffraction. Measurements of samples A–J (with sample A being the solid from the $Eu(NO_3)_3$-H_2O system, B–F are samples of the $Eu(NO_3)_3$-$NaNO_3$-H_2O system and G–J of the $Eu(NO_3)_3$-$Mg(NO_3)_2$-H_2O system; see Table 1 for detailed description) were performed in modified Si sample holders with cavity (1 mm depth) with an Empyrean diffractometer (Malvern Panalytical) using Cu-K_α radiation. A Bragg–Brentano HD device (Malvern Panalytical) was used to isolate the K_α from the K_β radiation and to reduce the fluorescence and the background. The primary optics included divergent slits (1/16°), anti-scattering slits (1/4°), mask 4 mm and soller slits (0.04 Rad). Detection was conducted by a multi-strip PIXcel 3D detector covering 3.348 °2θ simultaneously with 255 channels. The scan range was 5–90 °2θ with a 0.013 °2θ step size and 3.14 s per step.

Measurements of samples K–R (all samples of the $Eu(NO_3)_3$-$Mg(NO_3)_2$-H_2O system; see Table 1) were performed with a diffractometer D8 Advance (Bruker AXS) with a Lynxeye XE-T

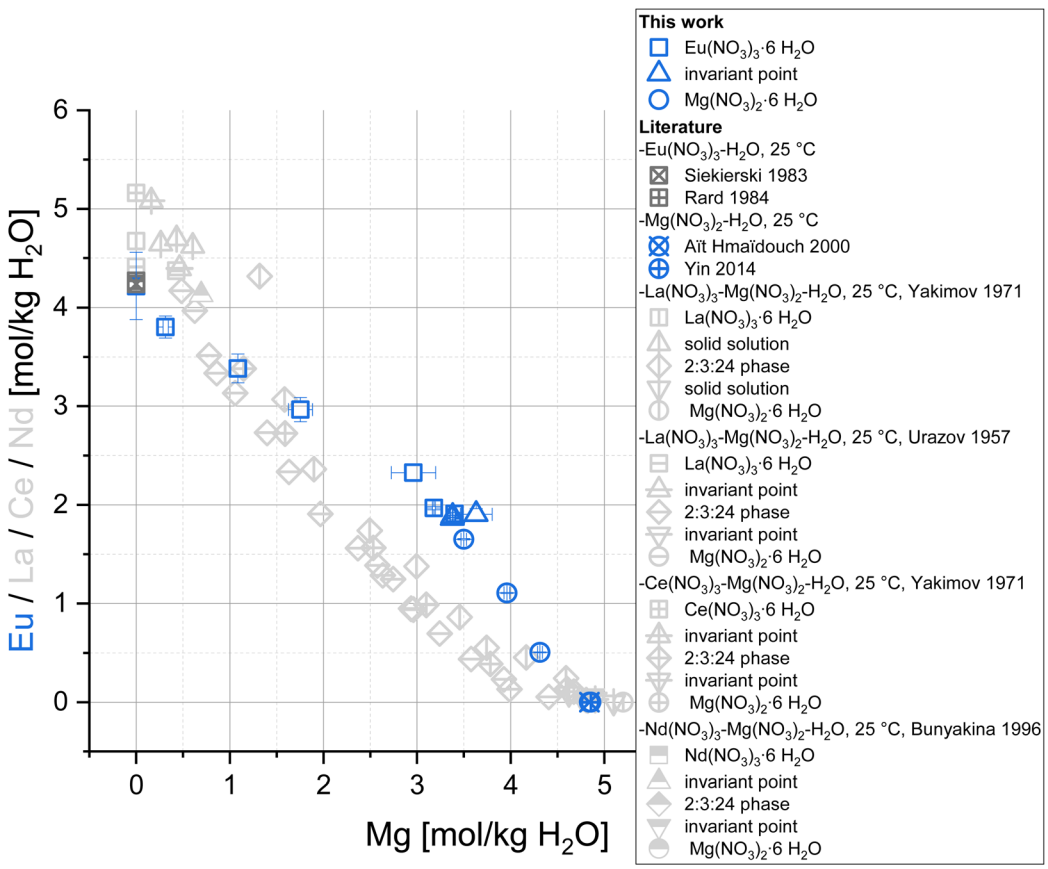

Fig. 2 Solubility data for the system $Eu(NO_3)_3$-$Mg(NO_3)_2$-H_2O (blue) at $T = (22 \pm 2)$ °C (complemented by literature data for solubilities in the binary subsystems at 25 °C [12,13,15,16]) compared to solubility data of the systems $La(NO_3)_3$-$Mg(NO_3)_2$-H_2O, $Ce(NO_3)_3$-$Mg(NO_3)_2$-H_2O, and $Nd(NO_3)_3$-$Mg(NO_3)_2$-H_2O (light grey).[53,55,56]

Table 2 Molalities m at set water activities a_w, and resulting osmotic coefficients φ in the systems $Eu(NO_3)_3$-$NaNO_3$-H_2O and $Eu(NO_3)_3$-$Mg(NO_3)_2$-H_2O at 25 °C. IWA: data obtained with the climatic chamber; DVS: data obtained with the DVS apparatus; experimental uncertainty for concentrations below ± 0.05 mol per kg H_2O

$Eu(NO_3)_3$-$NaNO_3$-H_2O

Sample	a_w	m($NaNO_3$) in mol per kg H_2O	m($Eu(NO_3)_3$) in mol per kg H_2O	φ
IWA-1	0.60	1.33	3.91	1.550
	0.70	1.07	3.14	1.345
	0.80	0.79	2.32	1.141
	0.60	1.32	3.89	1.557
IWA-2	0.70	2.70	2.72	1.217
	0.80	1.92	1.93	1.073
	0.60	3.45	3.47	1.365
IWA-3	0.80	4.05	1.36	0.914
	0.70	5.80	1.95	1.021
	0.68	6.04	2.03	1.060
DVS-1	0.80	0.72	2.13	1.245
	0.70	0.97	2.86	1.479
	0.60	1.26	3.70	1.637
	0.50	1.52	4.46	1.844
	0.60	1.26	3.71	1.632
	0.70	0.98	2.87	1.475
	0.80	0.74	2.17	1.222
DVS-2	0.80	1.93	1.94	1.064
	0.70	2.59	2.60	1.272
	0.60	3.44	3.46	1.367
	0.50	4.26	4.28	1.501
	0.60	3.48	3.50	1.352
	0.70	2.62	2.63	1.256
DVS-3	0.80	4.00	1.34	0.928
	0.70	5.55	1.86	1.067
	0.60	7.40	2.48	1.146
	0.70	5.71	1.92	1.037
	0.80	4.10	1.37	0.905

$Eu(NO_3)_3$-$Mg(NO_3)_2$-H_2O

Sample	a_w	m($Mg(NO_3)_2$) in mol per kg H_2O	m($Eu(NO_3)_3$) in mol per kg H_2O	φ
DVS-4	0.80	0.60	1.86	1.340
	0.70	0.79	2.45	1.627
	0.60	1.02	3.18	1.795
	0.50	1.24	3.83	2.021
	0.60	1.03	3.20	1.781
	0.70	0.80	2.47	1.612
	0.80	0.60	1.87	1.336
DVS-5	0.80	1.48	1.10	1.399
	0.70	1.95	1.45	1.702
	0.60	2.50	1.86	1.898
	0.50	2.99	2.22	2.158
	0.60	2.51	1.86	1.891
	0.70	1.96	1.45	1.691
	0.80	1.50	1.11	1.386
DVS-6	0.80	1.98	0.65	1.446
	0.70	2.58	0.85	1.777
	0.60	3.29	1.08	1.995
	0.50	3.90	1.29	2.281
	0.60	3.30	1.09	1.990
	0.70	2.59	0.85	1.772
	0.80	1.99	0.66	1.441

detector (1D mode) in Bragg–Brentano set-up using Cu-K_α radiation (the high energy resolution of 380 eV of the detector allows the selection of Cu-K_α radiation without an additional monochromator). A step size of 0.013 °2θ with 0.1–0.2 s per step was applied within the scan range of 5–60 °2θ.

The preparation of samples for measurement was kept as short as possible to prevent phase changes of the hygroscopic samples. A fraction of the solid phase was taken from the sample, roughly dried with absorbent paper and instantly prepared for measurement. Usually, three measurements of a sample were conducted in a row to identify time dependent phase changes and secondary crystallizations. The washing of samples with ethanol was tested, but resulted in high dissolution and subsequent crystallization, leading to a varying phase assemblage, which not necessarily represents equilibrium phases. Therefore, the former method without washing was preferred, despite the known disadvantages. A summary of XRPD measurements is presented in the SI of this work.

Rietveld refinement

Samples A–J have been evaluated and quantified by Rietveld refinement performed with TOPAS V.7 (Bruker-AXS, Karlsruhe, Germany). The structures of $Eu(NO_3)_3(H_2O)_6$ (ICSD 280528) and Eu $(NO_3)_3(H_2O)_4(H_2O)$ (ICSD 61257) were used as starting models for samples A–D and G–J.[23,24] For sample D, the structure of nitratine ($NaNO_3$, ICSD 14185) was additionally taken into account.[25] Samples E and F were refined using solely the structure of nitratine. The profile fitting was performed with the fundamental parameters approach (TOPAS V.7 Technical reference, Bruker-AXS) in the range 5–80 °2θ. The size of the coherent scattering domains was calculated by the double Voigt approach[26] implemented in TOPAS V.7.

Schreinemakers' method

Schreinemakers' method[27] was executed for the $Eu(NO_3)_3$-$Mg(NO_3)_2$-H_2O samples to verify phase compositions despite fast hygroscopicity effects of solid phases outside their mother liquor, which were observed during XRPD measurements. Fractions of each sample with varying liquid/solid ratios were weighted (79–281 mg) and afterwards dissolved in 10 mL 2% HNO_3. The resulting solutions were further diluted (1 : 250–1 : 500), followed by the analysis of Eu and Mg contents *via* ICP-OES as described earlier for the solubility experiments. Resulting compositions of suspensions and solutions were converted to mass fractions of $Eu(NO_3)_3$, $Mg(NO_3)_2$, and H_2O (the water content was calculated on the basis of Eu and Mg contents) and plotted in a ternary diagram to deduce the solid phases in equilibrium by extrapolation.

Thermodynamic modelling

The activities a_i (−) of solvent and solute describe the deviation from ideal behaviour induced by interactions in solution. For solutes, activity coefficients γ_i (−) quantify this deviation by

$$\gamma_i = \frac{a_i(\text{real})}{a_i(\text{ideal})} \quad (1)$$

which leads to the correlation of activity and the measurable molality of real solutions:

$$a_i(\text{real}) = \gamma_i \cdot \frac{m_i}{m_0} \quad (m_0 = 1 \text{ mol per kg } H_2O) \tag{2}$$

The solubility behaviour of solids is accordingly required to describe solid–liquid equilibria. For dissolution/precipitation processes, the following equation applies:

$$\Delta G = \Delta G^\circ + R \cdot T \cdot \ln \prod_i a_i^{\nu_i} \tag{3}$$

with ΔG – free energy change (which results 0 J mol^{-1} in thermodynamic equilibrium), ΔG° – standard free energy change, R – universal gas constant (8.314 J mol^{-1} K^{-1}), T – temperature in K and ν_i – stoichiometric coefficient (−) of species i. Solids are generally considered as pure phases, with constant unit activity. For thermodynamic equilibrium, the following further applies

$$\Delta G^\circ = -R \cdot T \cdot \ln K^\circ_{s,0} \tag{4}$$

where $K^\circ_{s,0}$ is the solubility constant (−) of a given solid phase. By combining eqn (3) and (4) one obtains:

$$\Delta G = R \cdot T \cdot \ln \frac{\prod_i a_i^{\nu_i}}{K^\circ_{s,0}} \tag{5}$$

$$\text{SR} = \frac{\prod_i a_i^{\nu_i}}{K^\circ_{s,0}} \tag{6}$$

The saturation ratio SR (−), defined as the quotient of ion activity product and solubility constant, equals 1 at equilibrium. For SR > 1 a solution would be supersaturated, while at SR < 1 it is undersaturated with respect to the solid. The saturation ratio is used in the present work to model the solubility curves and compare calculated and experimental values.

The activity of the solvent water, a_w, is also influenced by the interactions caused by dissolving salts. In contrast to activity coefficients of the electrolytes, the change for the activity coefficient of water is comparatively low in moderately concentrated solutions (relative to the electric charge of the solutes, and thus on the ionic strength). Thus, the numerically more sensitive osmotic coefficient φ (−) is usually used to quantify those changes according to Dinane:[28]

$$\varphi = -\frac{1000 \cdot \ln a_w}{M_w \cdot \sum_i \nu_i m_i} \tag{7}$$

with a_w – water activity, M_w – molar mass of water (18.02 g mol^{-1}), m_i – molality (mol per kg H_2O) of dissolved electrolyte i and ν_i – the number of ions produced by the total dissociation of electrolyte i. Osmotic coefficients are used in the present work to converge proposed models to the experimental results of IWA/DVS experiments.

An essential task in geochemical modelling of saline solutions is the description of ionic interactions, which gain relevance and complexity with increasing ionic strength. A basis for many models is the (extended) Debye–Hückel model, which is able to describe long-range interactions for very dilute solutions (<10^{-2}–10^{-1} mol per kg H_2O).[17,29–31] Higher ionic strengths demand the introduction of additional parameters to describe the increasing influence of short-range interactions. This is required especially at high molalities, which are certainly expected for nitrate salts.[12–16] The Pitzer model[17] is one of the most promising approaches for this purpose and is by now widely used in consistent thermodynamic databases[32,33] to describe high saline solutions. A brief summary of the Pitzer equations is given in the SI of F. dos Santos *et al.*[34] The reader is referred to the original Pitzer publications[17,18] for a more detailed description of these equations.

The present work is based on the full dissociation approach for dissolved salts considering Eu^{3+}, Na^+, Mg^{2+} and NO_3^- as aqueous species. Previous studies[30,35,36] showed good descriptions of solubility behaviour with the full dissociation assumption. In this way the semi-empirical parameters consider a possible formation of ion pairs or aqueous complexes as specific interactions without explicitly stating their existence. This drastically reduces the number of parameters needed and therefore reduces the present risk of overparameterization.

However, considering ion pairs and aqueous complexes enables a more realistic description of the chemical behaviour. Previous studies state the existence of europium nitrate[37,38] and sodium nitrate[39] complexes in solution. $MgNO_3^+$ seems also worth considering based on the description of various other MgX^+ ($X^- = F^-$, Cl^-, Br^-, I^-, HCO_3^-, …) and ANO_3^+ ($A^{2+} = Ca^{2+}$, Sr^{2+}, Ba^{2+}, Mn^{2+}, Ni^{2+}, …) aqueous species in the ThermoChimie[40] database (and references therein). The inclusion of complexes in SIT and Pitzer partial dissociation models is the main subject of future work.

Parametrization procedure

Modelling the solubility behaviour of aqueous ternary systems requires a consistent set of parameters, which, for a full dissociation Pitzer approach, includes the decadic logarithm of solubility constants at infinite dilution log $K^\circ_{s,0}$ of involved solids as well as specific binary ($\beta^{(0)}_{i,j}$, $\beta^{(1)}_{i,j}$, $\beta^{(2)}_{i,j}$, $C_{i,j}{}^{\phi}$) and ternary ($\theta_{i,k}$, $\Psi_{i,k,j}$) Pitzer interaction parameters (where i and k designate cations and j represents an anion).

The parametrization procedure is based on experimental solubility, DVS, and IWA data of the ternary systems $Eu(NO_3)_3$-$NaNO_3$-H_2O and $Eu(NO_3)_3$-$Mg(NO_3)_2$-H_2O (obtained in the present work) and interaction parameters for the binary subsystems $Eu(NO_3)_3$-H_2O, $NaNO_3$-H_2O, and $Mg(NO_3)_2$-H_2O, which were determined by Guignot *et al.*[41] and Lach *et al.*[42] In a first step, the binary parameters were tested within their respective systems against experimental literature data[43–49] and kept constant for the ternary systems to ensure consistency within the database. Additional needed cation interaction parameters θ_{Eu^{3+},Na^+} and $\theta_{Eu^{3+},Mg^{2+}}$ were taken from the work of F. dos Santos *et al.*[34] on the respective sulphate systems, while ternary parameters $\Psi_{Eu^{3+},Na^+,NO_3^-}$, and $\Psi_{Eu^{3+},Mg^{2+},NO_3^-}$ were determined in the present work. To do so, the parameter estimation software PEST[50] was coupled with the geochemical

calculation code PhreeSCALE[51] and its corresponding database[32] as earlier described in F. dos Santos *et al.*[34] New ternary parameters were estimated based on 70 data points from solubility and iso-water activity experiments of this work.

The optimization procedure aims at minimizing the deviation between the resulting models and the experimental data, which is described with sigma values, σ, as utilized in the work of Christov & Moller:[52]

$$\sigma = \sqrt{\frac{\sum_{i=1}^{n}\left(x(i)_{\mathrm{exp}} - x(i)_{\mathrm{calc}}\right)^2}{n}} \quad (8)$$

with the experimental and calculated values $x(i)_{\mathrm{exp}}$ and $x(i)_{\mathrm{calc}}$ for a data point i and n as the number of data points in the respective set. For solubility data (9) and osmotic coefficients (10) this leads to:

$$\sigma = \sqrt{\frac{\sum_{i=1}^{n}(\ln \mathrm{SR}(i))^2}{n}} \quad (9)$$

$$\sigma = \sqrt{\frac{\sum_{i=1}^{n}\left(\varphi(i)_{\mathrm{exp}} - \varphi(i)_{\mathrm{calc}}\right)^2}{n}} \quad (10)$$

Results and discussion

Solubility and iso-water activity data

The determined solubility data of the systems $Eu(NO_3)_3$-H_2O, $Eu(NO_3)_3$-$NaNO_3$-H_2O and $Eu(NO_3)_3$-$Mg(NO_3)_2$-H_2O at T = (22 ± 2) °C and pH ≤ 3.8 are listed in Table 1.

The solubility of $Eu(NO_3)_3 \cdot 6H_2O$ in water (4.22 ± 0.34 mol per kg H_2O) is in excellent agreement with literature values.[12,13] With this concentration baseline, the system $Eu(NO_3)_3$-$NaNO_3$-H_2O (Fig. 1, red symbols) shows a minor increase in Eu concentration up to 4.40 mol per kg H_2O with increasing $NaNO_3$ concentration. The solubility curve reaches an invariant point around 2.75 mol $NaNO_3$ per kg H_2O confirmed *via* XRPD by the simultaneous identification of both solid phases $Eu(NO_3)_3 \cdot 6H_2O$ and $NaNO_3$ in equilibrium with the solution (see Fig. 3 sample D in the next section). Starting from a pure Na-NO_3-H_2O system with $NaNO_3$ in equilibrium ($NaNO_3$ saturation at 10.79 mol per kg H_2O[14]), $NaNO_3$ remains the solid equilibrium phase with increasing the $Eu(NO_3)_3$ concentration until the invariant point (4.18 ± 0.18 mol $Eu(NO_3)_3$ per kg H_2O) is reached.

The observed trend of the $Eu(NO_3)_3$-$NaNO_3$-H_2O solubility curve is in good agreement with solubility data of the lanthanide systems $La(NO_3)_3$-$NaNO_3$-H_2O[53] and $Ce(NO_3)_3$-$NaNO_3$-H_2O[54] (Fig. 1, light grey symbols). Both show a similar increase in lanthanide (La or Ce) concentrations up to their respective invariant points between 1.73 and 2.42 mol $NaNO_3$ per kg H_2O,

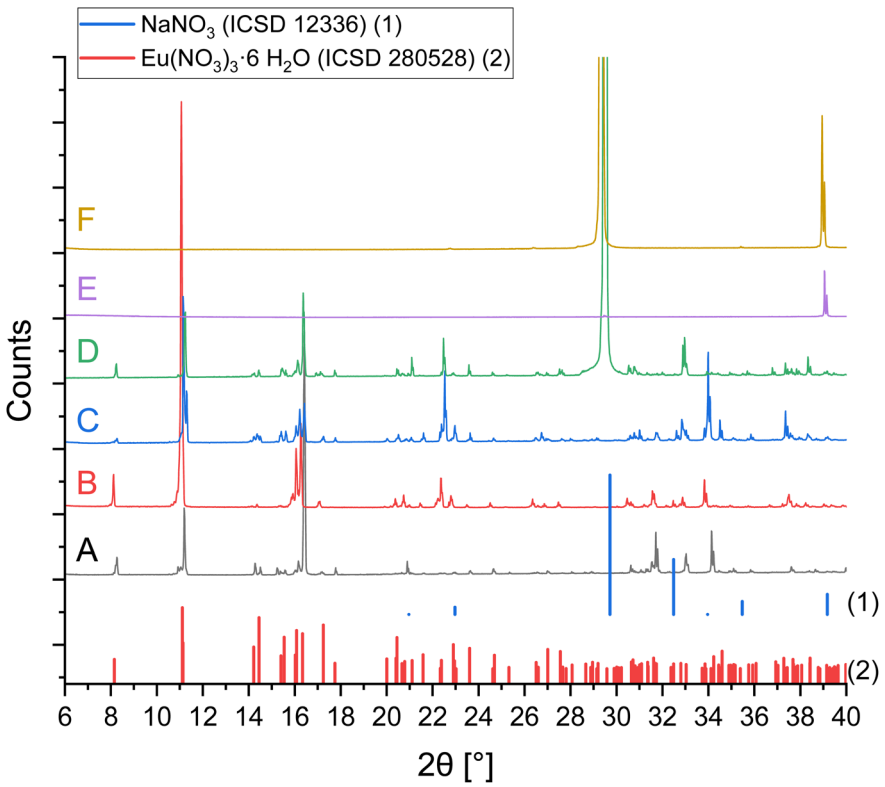

Fig. 3 X-ray powder diffraction patterns of the separated solid phases A–F from solubility investigations in the system $Eu(NO_3)_3$-$NaNO_3$-H_2O (0–5 mol $NaNO_3$ per kg H_2O) compared to reference lines.[23,60]

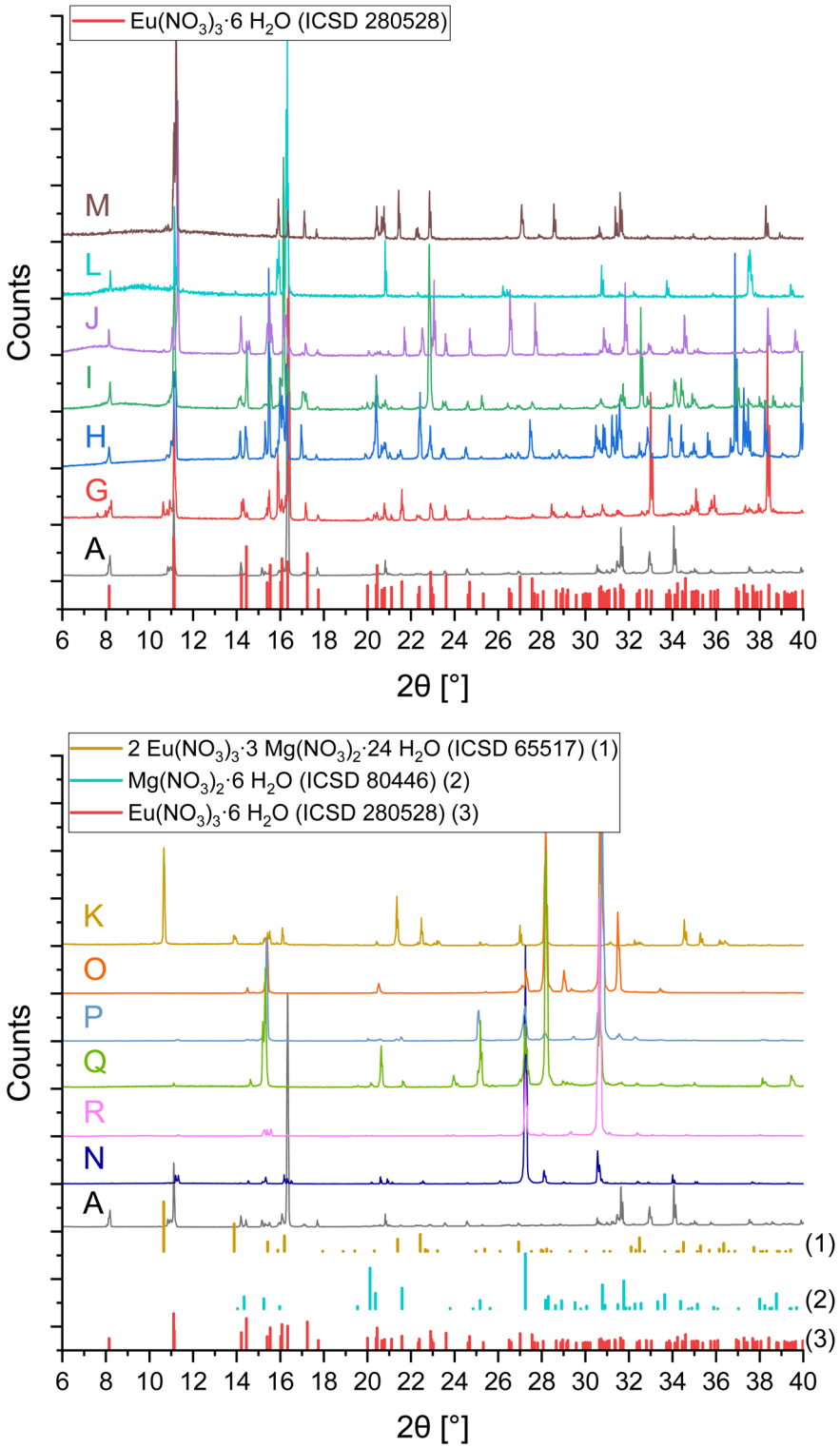

Fig. 4 X-ray powder diffraction patterns of the separated solid phases A and G–R from solubility investigations in the system $Eu(NO_3)_3$-$Mg(NO_3)_2$-H_2O (0–4.3 mol $Mg(NO_3)_2$ per kg H_2O) compared to reference lines;[23,57,61] top: $Eu(NO_3)_3 \cdot 6H_2O$ dominated samples (≤3.4 mol $Mg(NO_3)_2$ per kg H_2O in solution), bottom: $Mg(NO_3)_2 \cdot 6H_2O$ dominated samples (≥3.4 mol $Mg(NO_3)_2$ per kg H_2O in solution); slight 2θ-shifts are executed for better illustration and comparison among the patterns (unmodified and time dependent XRPD results are included in the SI).

followed by a continuous decrease in lanthanide concentration with increasing $NaNO_3$ concentrations as observed for the $Eu(NO_3)_3$-$NaNO_3$-H_2O system in this work.

In the case of the $Eu(NO_3)_3$-$Mg(NO_3)_2$-H_2O system (Fig. 2, blue symbols), Eu concentrations, starting at 4.22 mol per kg H_2O in the binary $Eu(NO_3)_3$-H_2O system, decrease continuously with increasing $Mg(NO_3)_2$ concentration up to 4.84–4.86 mol

Table 3 Composition (in mass fraction) of samples for determination of solid phases in the system $Eu(NO_3)_3$-$Mg(NO_3)_2$-H_2O at $T = (22 \pm 2)$ °C using Schreinemakers' method; corresponding mass fractions of water were calculated based on these values

	Solution		Suspension 1 (low solid/liquid ratio)		Suspension 2 (high solid/liquid ratio)	
Sample	$Eu(NO_3)_3$	$Mg(NO_3)_2$	$Eu(NO_3)_3$	$Mg(NO_3)_2$	$Eu(NO_3)_3$	$Mg(NO_3)_2$
G	0.551 ± 0.005	0.020 ± 0.002	0.571 ± 0.011	0.018 ± 0.001	0.621 ± 0.009	0.014 ± 0.001
H	0.496 ± 0.011	0.070 ± 0.005	0.507 ± 0.008	0.062 ± 0.002	0.562 ± 0.008	0.055 ± 0.001
I	0.443 ± 0.007	0.115 ± 0.008	0.443 ± 0.003	0.108 ± 0.002	0.598 ± 0.010	0.062 ± 0.001
J	0.354 ± 0.009	0.197 ± 0.016	0.428 ± 0.015	0.15 ± 0.0060	0.494 ± 0.006	0.123 ± 0.003
K	0.295 ± 0.009	0.247 ± 0.012	0.308 ± 0.004	0.250 ± 0.006	0.322 ± 0.003	0.282 ± 0.004
			0.369 ± 0.002	0.252 ± 0.002	0.058 ± 0.001	0.472 ± 0.005
L	0.311 ± 0.003	0.221 ± 0.001	0.558 ± 0.009	0.102 ± 0.001	0.623 ± 0.002	0.081 ± 0.001
M	0.300 ± 0.003	0.235 ± 0.001	0.534 ± 0.003	0.116 ± 0.001	0.597 ± 0.003	0.087 ± 0.001
N	0.298 ± 0.002	0.235 ± 0.002	0.458 ± 0.002	0.167 ± 0.002	0.550 ± 0.002	0.112 ± 0.001
O	0.094 ± 0.001	0.353 ± 0.002	0.061 ± 0.001	0.419 ± 0.003	0.039 ± 0.001	0.461 ± 0.002
P	0.191 ± 0.001	0.300 ± 0.002	0.101 ± 0.001	0.413 ± 0.004	0.081 ± 0.002	0.429 ± 0.004
Q	0.269 ± 0.001	0.250 ± 0.002	0.181 ± 0.001	0.350 ± 0.006	0.118 ± 0.001	0.400 ± 0.001
R	0.296 ± 0.002	0.235 ± 0.002	0.337 ± 0.003	0.243 ± 0.002	0.375 ± 0.003	0.235 ± 0.004

$Mg(NO_3)_2$ per kg H_2O[15,16] (saturation concentration of $Mg(NO_3)_2$ in its binary aqueous system). The course of the solubility curve indicates an invariant point of $Eu(NO_3)_3 \cdot 6H_2O$ and $Mg(NO_3)_2 \cdot 6H_2O$ at *ca.* 3.4 mol per kg H_2O $Mg(NO_3)_2$, which overall agrees well with the solid phase analyses by XPRD and Schreinemakers' method (see next section). The formation of $2Eu(NO_3)_3 \cdot 3Mg(NO_3)_2 \cdot 24H_2O$ is not evident based on the solubility investigation. This double salt was found in the XRPD pattern of sample K, but cannot be confirmed with

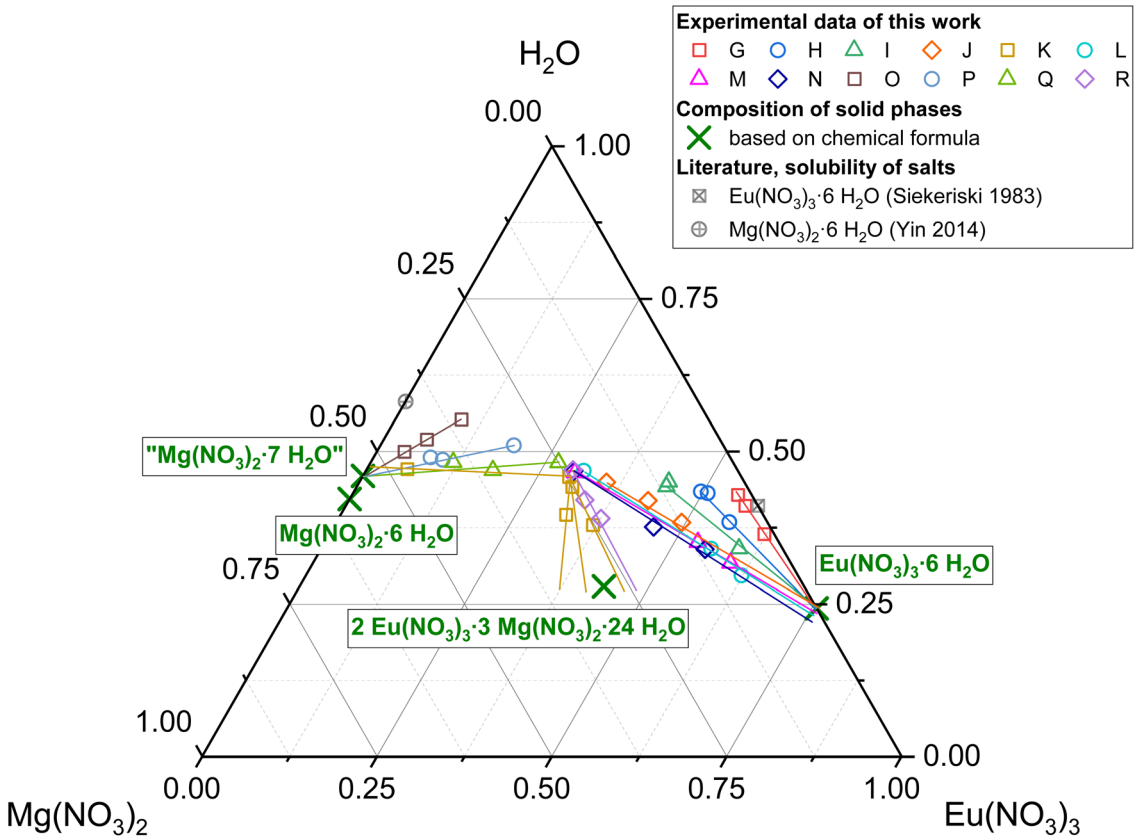

Fig. 5 Schreinemakers' method to determine the composition of solid phases in equilibrium with the solutions of samples G–R in the system $Eu(NO_3)_3$-$Mg(NO_3)_2$-H_2O (see Table 3); data points of the same sample are illustrated in the same colour and include compositions of separated solutions and suspensions with different solid/liquid ratios, lines are added manually for illustration; grey symbols represent literature solubility data[12,16] of $Mg(NO_3)_2 \cdot 6H_2O$ and $Eu(NO_3)_3 \cdot 6H_2O$ at 25 °C in their respective binary aqueous systems.

Schreinemakers' method. A discussion on this disagreement is provided in the next chapter.

The observed solubility behaviour is significantly different compared to the systems $La(NO_3)_3$-$Mg(NO_3)_2$-H_2O,[53] $Ce(NO_3)_3$-$Mg(NO_3)_2$-H_2O,[55] and $Nd(NO_3)_3$-$Mg(NO_3)_2$-H_2O[56] in which the formation of $2Ln(NO_3)_3 \cdot 3Mg(NO_3)_2 \cdot 24H_2O$ (Ln = La, Ce, Nd) dominates between 0.5 and 4.5 mol $Mg(NO_3)_2$ per kg H_2O (Fig. 2, light grey symbols). Akimov *et al.*[57] described the formation of the equivalent Eu phase at room temperature from an $Eu(NO_3)_3$-$Mg(NO_3)_2$ solution (concentrations not specified) in 6 molar nitric acid and determined its crystal structure. Qiao *et al.*[58] investigated phase equilibria in the comparatively acidic (6.2–7.8 mol HNO_3 per kg H_2O) quaternary $Ln(NO_3)_3$-$Mg(NO_3)_2$-HNO_3 (20 w%)-H_2O systems (Ln = Nd, Sm, Eu, Tb) and reported the formation of $2Ln(NO_3)_3 \cdot 3Mg(NO_3)_2 \cdot 24H_2O$ in case of Ln = Nd and Sm but not for Ln = Eu and Tb, based on results of Schreinemakers' method. A significant difference compared to the present work are the high HNO_3 concentrations in both literature experiments.[57,58] Comparable solubility studies for the ternary system $Eu(NO_3)_3$-$Mg(NO_3)_2$-H_2O are not available in the literature, to the best of our knowledge. Based on the overall results, $2Eu(NO_3)_3 \cdot 3Mg(NO_3)_2 \cdot 24H_2O$ is assumed to be a metastable phase compared to the single salts in the $Eu(NO_3)_3$-$Mg(NO_3)_2$-H_2O system with its solubility curve closely passing by the invariant point of $Eu(NO_3)_3 \cdot 6H_2O$ and $Mg(NO_3)_2 \cdot 6H_2O$. In fact, Eu seems to be a "transition point" within the $Ln(NO_3)_3$-$Mg(NO_3)_2$-H_2O system series, for which the $2Ln(NO_3)_3 \cdot 3Mg(NO_3)_2 \cdot 24H_2O$ phase is described as a stable phase over large concentration ranges for lanthanides lighter than Eu, while it is not described as such for heavier ones.

The pH values of all solutions were determined after the last sampling and resulted consequently in values of pH ≤ 3.8. The hydrolysis of Eu(III) is not expected to play a major role under these conditions as shown by Jordan *et al.*[59] for the aqueous Eu(III) hydroxide system. Consequently, Eu^{3+} and Eu(III)-nitrato complexes are expected as dominant aqueous Eu(III) species.

Another set of samples was prepared to determine osmotic coefficients at set water activities. Table 2 contains molalities of the involved salts in the ternary systems $Eu(NO_3)_3$-$NaNO_3$-H_2O and $Eu(NO_3)_3$-$Mg(NO_3)_2$-H_2O. The values were determined by measuring the weight differences for each sample (different initial salt molalities), resulting from equilibration at selected relative humidities RH_{eq} $\left(a_W = \frac{RH_{eq}}{100}\right)$. The osmotic coefficients φ were calculated according to eqn (7). The osmotic coefficient values increase with decreasing relative humidity and show reproducibility confirming equilibrium state.

Solid phase characterization

X-ray powder diffraction was used for solid phase characterization of samples from the solubility experiments. The investigated solid samples A–R are indicated in Table 1. Fig. 3 shows the XRPD patterns for samples A–F of the system $Eu(NO_3)_3$-$NaNO_3$-H_2O. Sample A does not contain any $NaNO_3$, thus the only solid phase in equilibrium is $Eu(NO_3)_3 \cdot 6H_2O$. With rising $NaNO_3$ concentration in samples B and C, $Eu(NO_3)_3 \cdot 6H_2O$ still remains the solid phase in equilibrium. The diffraction pattern of sample D (m($NaNO_3$) = 2.75 mol per kg H_2O) contains signals of both $Eu(NO_3)_3 \cdot 6H_2O$ and $NaNO_3$, which is consistent with

Table 4 Parameters used for modelling the systems $Eu(NO_3)_3$-$NaNO_3$-H_2O and $Eu(NO_3)_3$-$Mg(NO_3)_2$-H_2O at 25 °C in this work

Pitzer parameters binary systems

Species i	Species j	$\alpha_{1/2}$	$\beta^{(0)}_{i,j}$	$\beta^{(1)}_{i,j}$	$\beta^{(2)}_{i,j}$	$C_{i,j}{}^{\phi}$	References
Eu^{3+}	NO_3^-	2/0.6424	0.2669	3.5169	0.7029	−0.0072	Guignot *et al.*[41]
Na^+	NO_3^-	—	0.0038	0.1835	—	0	Lach *et al.*[42]
Mg^{2+}	NO_3^-	—	0.3286	1.9159	—	−0.0064	Lach *et al.*[42]

Pitzer parameters ternary systems

Species i	Species j	Species k	$\theta_{i,k}$	$\Psi_{i,k,j}$	References
Eu^{3+}	NO_3^-	Na^+	0.2223*	−0.017**	*F. dos Santos *et al.*[34] **This work
Eu^{3+}	NO_3^-	Mg^{2+}	−0.182*	0.017**	*F. dos Santos *et al.*[34] **This work

Solubility constants

Solid phase	log $K^{\circ}_{s,0}$	References
$Eu(NO_3)_3\ 6H_2O \rightleftarrows Eu^{3+} + 3NO_3^- + 6H_2O$	1.8617	Guignot *et al.*[41]
$NaNO_3 \rightleftarrows Na^+ + NO_3^-$	1.0864	Lach *et al.*[42]
$Mg(NO_3)_2 \cdot 6H_2O \rightleftarrows Mg^{2+} + 2NO_3^- + 6H_2O$	3.05	Lach *et al.*[42]

the observed invariant point in the solubility curve. A further increase in $NaNO_3$ solution concentrations up to 5 mol per kg H_2O leads to the sole formation of $NaNO_3$, which is the solid phase in equilibrium in samples E and F. These XRPD-results complement the progression of the solubility data in Fig. 1 well.

The XRPD patterns for samples of the system $Eu(NO_3)_3$-$Mg(NO_3)_2$-H_2O are illustrated in Fig. 4 in comparison to sample A. The patterns in the upper part (samples G–J, L, M) can be described with the $Eu(NO_3)_3 \cdot 6H_2O$ reference lines.[23] The XRPD patterns in the lower part of Fig. 4 (samples K and O–R) are distinctly different, which indicates a solid phase change in solutions with ≥3.4 mol $Mg(NO_3)_2$ per kg H_2O (stated invariant point based on the determined solubility curve).

The diffraction patterns of samples N–R are best explained by $Mg(NO_3)_2 \cdot 6H_2O$ reference lines.[61] The presence of $Eu(NO_3)_3 \cdot 6H_2O$ is expected for samples N and R based on the composition of their corresponding solutions, but is in the XRPD patterns just indicated by minor signals. Solution compositions of samples O, P and Q are on the assumed $Mg(NO_3)_2 \cdot 6H_2O$-branch of the solubility curve, where $Mg(NO_3)_2 \cdot 6H_2O$ should be the solid phase in equilibrium, which is consistent with the X-ray diffraction patterns.

The XRPD pattern of sample K (10.7 °2θ, 21.4 °2θ, and 22.4 °2θ, …) can best be explained by $2Eu(NO_3)_3 \cdot 3Mg(NO_3)_2 \cdot 24H_2O$ reference lines.[57] Based on the solubility experiments, this is expected to be a metastable phase compared to the simple Eu- and Mg-nitrate salts, since the corresponding solution of this sample is supersaturated compared to the systematic solubility curve which results from the solution compositions of all other samples. This indicates that the formation is also the result of a, at least local, oversaturation. Note however that a phase transformation of this once formed 2:3:24 phase in sample K was not observed in the course of these experiments (up to 2 years). This might be due to kinetic inhibition but is not clear for the time being, and should be further investigated in the future. The presence of $Mg(NO_3)_2 \cdot 6H_2O$ cannot be excluded based on the XRPD results, due to the overlap of some reference lines.

XRPD measurements overall provided some experimental challenges. Different attempts of washing the solid phases (with water or ethanol) resulted in phase changes and dissolution due to high solubility of nitrates. Strong hygroscopic effects led to dissolution of initially dried samples during longer measurements. Thus, comparatively short measurements of roughly crushed crystals with adherent mother liquor were executed to qualitatively analyse the solids, before any phase change. This results in signal displacements and missing signals due to preferential crystal orientations (Fig. 4). However, the results still provide valuable information on the solid phases.

Rietveld refinements were conducted for samples A–J. Resulting compositions are listed in Table 1, while refined unit cell parameters, sizes of coherent scattering domains, and all Rietveld plots can be found in the SI. For samples with

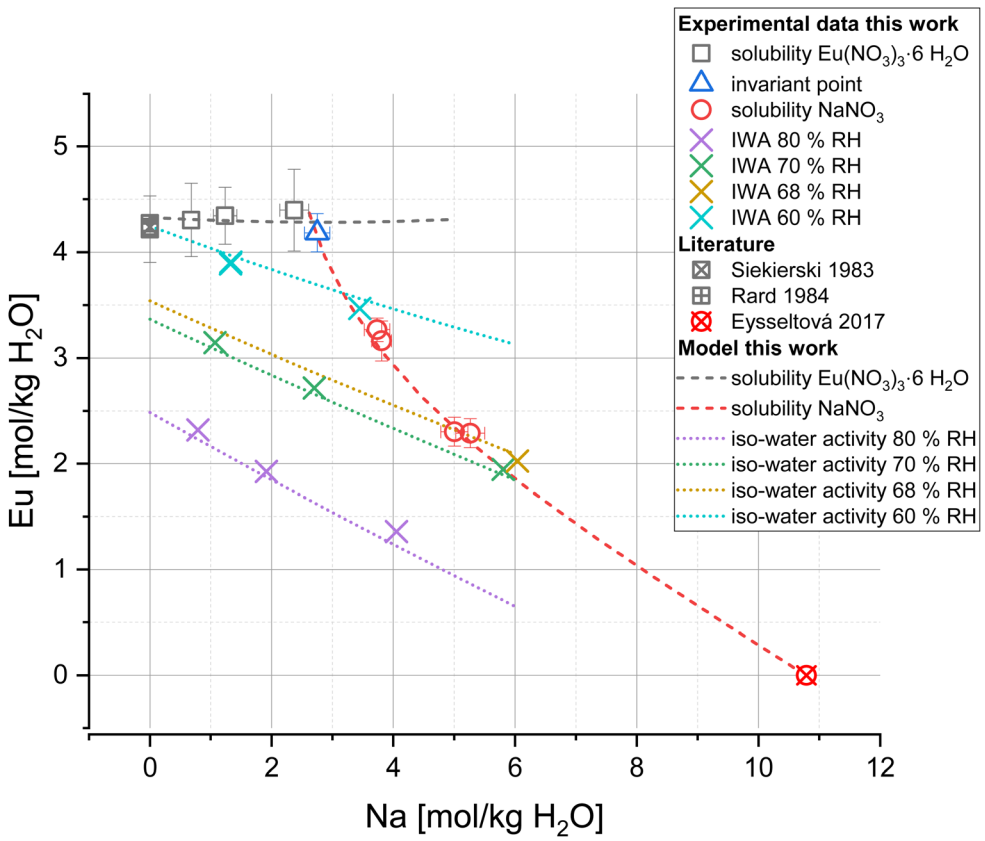

Fig. 6 $Eu(NO_3)_3$-$NaNO_3$-H_2O solubility and iso-water activity curves at 25 °C calculated with PhreeSCALE (lines) compared to experimental data of this work and literature[12–14] (symbols).

the equilibrium phase $Eu(NO_3)_3 \cdot 6H_2O$ (A–D, G–J) it was shown that despite $Eu(NO_3)_3 \cdot 6H_2O$ being the main phase, $Eu(NO_3)_3(H_2O)_4(H_2O)$ was always found in varying amounts. This indicates a secondary phase change during sample preparation and XRD measurement. Both phases are quite similar and show strong orientation. $NaNO_3$ was found in samples D–F, identified with *ca.* 17 wt% in sample D (invariant point of the solubility curve; the theoretical ratio of $NaNO_3$ in a 1 : 1 mixture with $Eu(NO_3)_3 \cdot 6H_2O$ is 16 wt%), while being the only solid in equilibrium for samples E and F.

Because of the experimental issues for XRPD and the uncertainties coming with them for the $Eu(NO_3)_3$-$Mg(NO_3)_2$-H_2O system, solid phase compositions were additionally analysed by Schreinemakers' method,[27] in which the composition of solid phases is graphically deduced based on the composition of the solution in equilibrium and corresponding suspensions. At least three points were determined per sample to provide more analytical accuracy despite the high dilutions necessary for analysis. Results are listed in Table 3 and illustrated in Fig. 5.

$Eu(NO_3)_3 \cdot 6H_2O$ can be identified as solid phase in equilibrium for samples G–J, L, and M, which agrees well with the results of XRPD (Fig. 4 top). Furthermore, it becomes evident that the solid phase in equilibrium with samples O, P and Q is a magnesium nitrate hydrate. Considering the present analytical uncertainty and the XRPD results, it is reasonable to assign $Mg(NO_3)_2 \cdot 6H_2O$ rather than $Mg(NO_3)_2 \cdot 7H_2O$, despite deviation from its exact hydration water content.

The results of the remaining samples N, R and K do not seem to describe a single solid phase, but a mixture of solids, which agrees with their solution compositions close to the postulated invariant point of the solubility curve. For samples N and R, a mixture of $Mg(NO_3)_2 \cdot 6H_2O$ and $Eu(NO_3)_3 \cdot 6H_2O$ is deduced based on the location of their data points comparatively close to $Eu(NO_3)_3 \cdot 6H_2O$ in combination with the identification of $Mg(NO_3)_2 \cdot 6H_2O$ in the XRPD patterns. The presence of $2Eu(NO_3)_3 \cdot 3Mg(NO_3)_2 \cdot 24H_2O$ was already shown for sample K by XRPD investigations. The scattering of its data points in Schreinemakers' method is based on varying ratios of different solids in the different samplings, which is most likely $Mg(NO_3)_2 \cdot 6H_2O$ besides $2Eu(NO_3)_3 \cdot 3Mg(NO_3)_2 \cdot 24H_2O$.

Thermodynamic modelling

The parameters required for the full dissociation models of the ternary systems $Eu(NO_3)_3$-$NaNO_3$-H_2O and $Eu(NO_3)_3$-$Mg(NO_3)_2$-H_2O are summarized in Table 4. Pitzer parameters for the binary systems $Eu(NO_3)_3$-H_2O, $Mg(NO_3)_2$-H_2O, and $NaNO_3$-H_2O as well as corresponding solubility constants $\log K^{\circ}_{s,0}$ are already established in the PhreeSCALE database.[32] They are taken from the works of Guignot *et al.*[41] and Lach *et al.*,[42] which provide comprehensive reviews on existing data as well as model attempts and present parameter sets most suitable for describing mean activity coefficients and osmotic coefficients at all concentrations up to saturation.

In order to describe the ternary systems properly, further Pitzer parameters $\theta_{i,k}$ and $\Psi_{i,k,j}$ need to be added. These

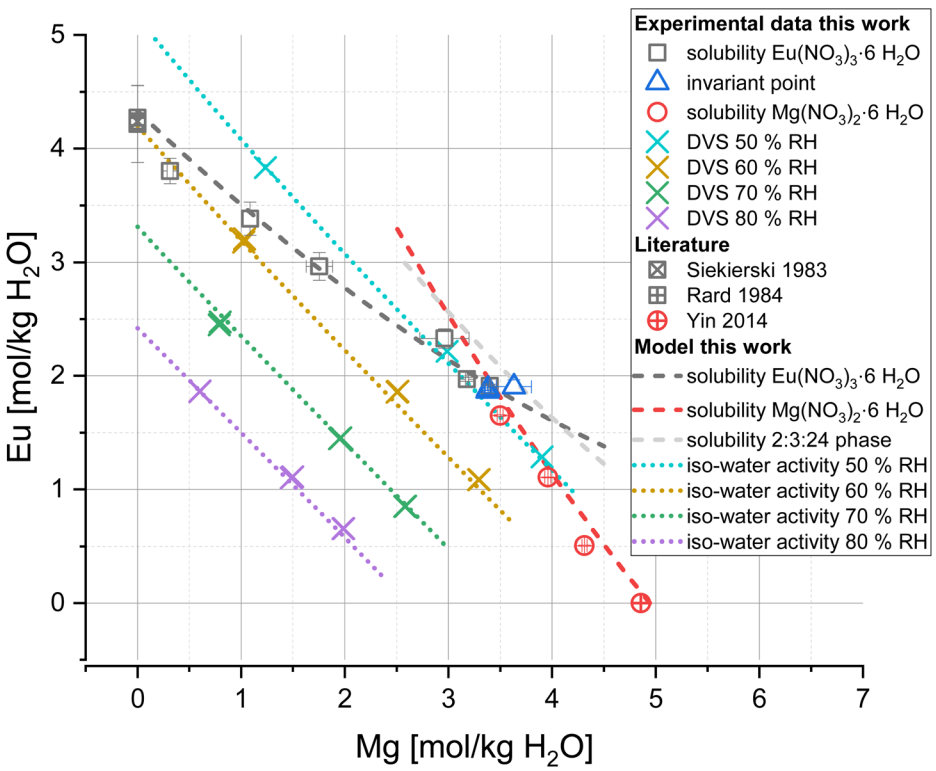

Fig. 7 $Eu(NO_3)_3$-$Mg(NO_3)_2$-H_2O solubility and iso-water activity curves at 25 °C calculated with PhreeSCALE (lines) compared to experimental data of this work and literature[12,13,15,16] (symbols).

describe interactions of the different cations i and k (Eu^{3+} and Na^{+} or Mg^{2+}) as well as the ternary interactions between cations i and k with the anion j (NO_3^-). The parameters $\theta_{i,k}$ were taken from the recent work of F. dos Santos *et al.*,[34] which provides full dissociation Pitzer models for the equivalent sulphate systems. The parameter sets were completed by determining the $\Psi_{i,k,j}$ parameters in this work, based on the presented experimental data.

Fig. 6 shows the solubility and iso-water activity data (symbols) compared to the model calculations (lines) for the system $Eu(NO_3)_3$-$NaNO_3$-H_2O. The modelled solubility curves reproduce the experimental values within the experimental uncertainties including the location of the invariant point $Eu(NO_3)_3$-$NaNO_3$ at 2.75 mol $NaNO_3$ per kg H_2O. The calculated iso-water activity curves are also in good agreement with the experimental results, illustrating the linear correlation at each relative humidity. The respective sigma values of 0.071 for solubility data and 0.084 for osmotic coefficients further indicate an overall good match between model and experimental results.

The comparison of experiments and the full dissociation Pitzer model for the system $Eu(NO_3)_3$-$Mg(NO_3)_2$-H_2O is shown in Fig. 7. An overall good agreement between experimental and calculated results is given for iso-water activity and solubility data (sigma values of 0.053 and 0.141, respectively). The linear trend of the iso-water activity data was reproduced for all investigated relative humidities. The solubility data of $Eu(NO_3)_3 \cdot 6H_2O$ and $Mg(NO_3)_2 \cdot 6H_2O$ are also properly reproduced including their invariant point around 3.4 mol $Mg(NO_3)_2$ per kg H_2O. Based on the presence of metastable $2Eu(NO_3)_3 \cdot 3Mg(NO_3)_2 \cdot 24H_2O$ in sample K, an additional solubility curve for this ternary 2:3:24 phase (Fig. 7, grey line) was calculated based on an estimated solubility product, *i.e.*, $\log K^{\circ}_{s,0} = 15.5$. Note that this value does not represent equilibrium conditions and should not be further implemented in thermodynamic databases.

Zalupski *et al.*[44] presented a large set of osmotic coefficients at 25 °C for the system $Eu(NO_3)_3$-$NaNO_3$-H_2O (up to 1 mol Eu per kg H_2O and 1.5 mol Na per kg H_2O), which is also reproduced by the presented model in very good approximation ($\sigma(\varphi) = 0.008$; see Fig. SI-20 in the SI). It should be mentioned that they introduced their own set of binary and ternary Pitzer parameters (comparable in magnitude to the binary and ternary parameters in Table 4). Although it describes their osmotic coefficients well, the parameters in Table 4 were preferred within the scope of this work to cover a larger concentration

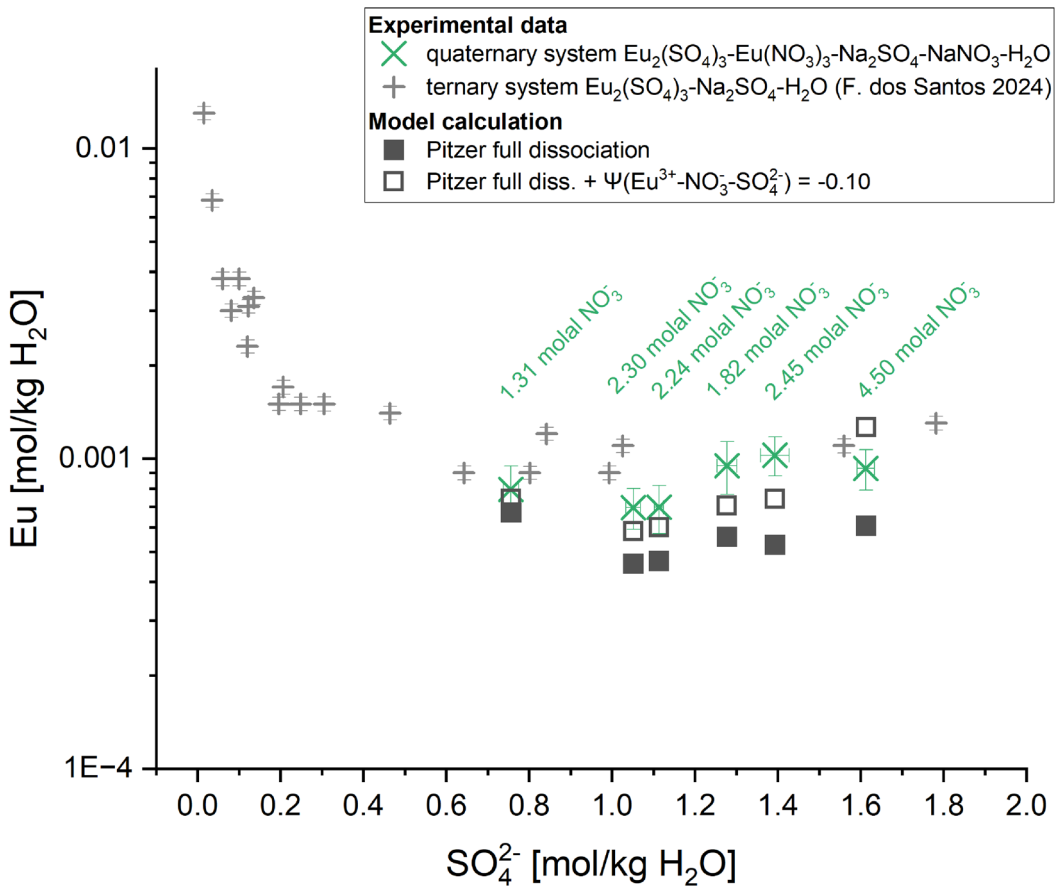

Fig. 8 Eu solubility data at 25 °C in the system $Eu_2(SO_4)_3$-$Eu(NO_3)_3$-Na_2SO_4-$NaNO_3$-H_2O calculated with PhreeSCALE (full black squares) compared to experimental data of this work (green crosses; NO_3^- concentrations labelled at each point); open symbols show the same calculations with the introduction of $\Psi_{Eu^{3+},NO_3^-,SO_4^{2-}} = -0.1$ to illustrate the impact of this currently unknown parameter on calculations in the quaternary system; grey crosses show experimental solubility data from the ternary system $Eu_2(SO_4)_3$-Na_2SO_4-H_2O (F. dos Santos *et al.*[34]).

Table 5 Solubility data for the quaternary system $Eu_2(SO_4)_3$-$Eu(NO_3)_3$-Na_2SO_4-$NaNO_3$-H_2O at $T = (22 \pm 2)$ °C; NO_3^- values are calculated based on weigh-ins under the assumption of full nitrate solubility and complete formation of $NaEu(SO_4)_2 \cdot H_2O$

Sample	Eu^{3+} in mmol per kg H_2O	Na^+ in mol per kg H_2O	SO_4^{2-} in mol per kg H_2O	NO_3^- in mol per kg H_2O
1	0.80 ± 0.15	2.78 ± 0.06	0.76 ± 0.02	1.31
2	0.70 ± 0.10	4.34 ± 0.05	1.05 ± 0.02	2.30
3	0.70 ± 0.12	4.47 ± 0.07	1.11 ± 0.01	2.24
4	1.03 ± 0.15	5.17 ± 0.14	1.39 ± 0.03	2.45
5	0.93 ± 0.14	7.55 ± 0.07	1.61 ± 0.02	4.50
6	0.95 ± 0.18	4.33 ± 0.03	1.28 ± 0.02	1.82

range of Eu and Na, and to keep consistency within the used database.

Lassin *et al.*[62] determined interaction parameters $\theta_{i,k}$ and $\Psi_{i,k,j}$ (based on solubility data published in Silcock *et al.*[63]) for related ternary lanthanide-nitrate systems $Cm(NO_3)_3$-$NaNO_3$-H_2O ($\theta_{Cm^{3+},Na^+} = 0.16623$ and $\Psi_{Cm^{3+},Na^+,NO_3^-} = -0.00936$) and $La(NO_3)_3$-$Mg(NO_3)_2$-H_2O ($\theta_{La^{3+},Mg^{2+}} = -0.68470$ and $\Psi_{La^{3+},Mg^{2+},NO_3^-} = 0.00501$), which are in a comparable magnitude to the parameters of this work for the respective Eu systems.

The presented parameter set is proposed as an addition to the PhreeSCALE database for the description of ternary Eu(III)–nitrate systems. It continues a series started with the respective Eu(III)–sulphate systems[34,64] to enable a thermodynamic description of high saline Ln(III)/An(III)–sulphate–nitrate systems. Additional solubility experiments were conducted within the quaternary system $Eu_2(SO_4)_3$-$Eu(NO_3)_3$-Na_2SO_4-$NaNO_3$-H_2O to test the progress to this point. The experiments included six samples with varying sulphate and nitrate contents to cover a wide concentration range. The resulting Eu concentrations are plotted against sulphate concentrations in Fig. 8 (results are listed in Table 5). In comparison, calculations using the PhreeSCALE database with the additional parameters of the full dissociation Pitzer models for the ternary systems $Eu_2(SO_4)_3$-Na_2SO_4-H_2O (F. dos Santos *et al.*[34]) and $Eu(NO_3)_3$-$NaNO_3$-H_2O (this work) are presented (full squares).

The calculated solid phase in equilibrium within the investigated sulphate concentration range is the double salt $NaEu(SO_4)_2 \cdot H_2O$, which agrees well with the results of F. dos Santos *et al.*[34] at the sulphate concentrations investigated in this work. The current model results in slightly lower Eu(III) concentrations at the given sodium nitrate and sulphate concentrations compared to the experimental data. The fit can be improved by introducing the missing ternary parameter $\Psi_{Eu^{3+},NO_3^-,SO_4^{2-}}$, which describes the interactions between the cation Eu^{3+} and the anions NO_3^- and SO_4^{2-} (interfering anion interactions with Eu^{3+} or competitive influence of the anions on Eu^{3+}). Introducing this parameter directly influences the Eu concentration in the quaternary system (exemplified for $\Psi_{Eu^{3+},NO_3^-,SO_4^{2-}} = -0.1$; open symbols in Fig. 8). The value of $\Psi_{Eu^{3+},NO_3^-,SO_4^{2-}}$ determined in this work should be considered as tentative due to the limited dataset available (6 experimental points). Future dedicated studies on the ternary system $Eu_2(SO_4)_3$-$Eu(NO_3)_3$-H_2O resulting in comprehensive datasets should be the basis for an accurate determination of this parameter.

Summary and conclusions

Solubility experiments in the ternary systems $Eu(NO_3)_3$-$NaNO_3$-H_2O and $Eu(NO_3)_3$-$Mg(NO_3)_2$-H_2O were conducted at $T = (22 \pm 2)$ °C over concentrations ranges of 0.0–5.3 mol $NaNO_3$ per kg H_2O and 0.0–4.3 mol $Mg(NO_3)_2$ per kg H_2O in weakly acidic solutions. Solid phase characterization was performed by X-ray powder diffraction and Schreinemakers' method. $Eu(NO_3)_3 \cdot 6H_2O$ and $NaNO_3$ were the only solid phases identified over the complete concentration range in the case of $Eu(NO_3)_3$-$NaNO_3$-H_2O. The invariant point observed in the solubility curve at 2.75 mol $NaNO_3$ per kg H_2O was confirmed by XRPD. $Eu(NO_3)_3 \cdot 6H_2O$ and $Mg(NO_3)_2 \cdot 6H_2O$ are defined as the only thermodynamically stable phases in the $Eu(NO_3)_3$-$Mg(NO_3)_2$-H_2O system. Solubility experiments and XRPD confirm the presence of an invariant point at *ca.* 3.4 mol $Mg(NO_3)_2$ per kg H_2O. The formation of $2Eu(NO_3)_3 \cdot 3Mg(NO_3)_2 \cdot 24H_2O$ was observed in one sample with a solution composition close to this invariant point, but this phase is considered as metastable at $T = (22 \pm 2)$ °C. Additional iso-water activity experiments at $T = 25$ °C were performed for a better characterization of ion interactions in solution by determining osmotic coefficients at fixed relative humidities (50–80% RH) for both ternary systems.

These results enabled the determination of a new set of Pitzer interaction parameters, which accurately describes solubility and iso-water activity data of both investigated systems at $T = 22$–25 °C and within the solubility limits of the corresponding salts. Based on the solubility constants and binary interaction parameters already implemented in PhreeSCALE[32] we derived missing ternary $\Psi_{i,k,j}$ parameters with the help of 70 new experimental data points, consistently with the $\theta_{i,k}$ cation–cation interaction parameters determined earlier by F. dos Santos *et al.*[34] Although out of the scope of this work, the need of extending the current model to elevated temperatures ($T \leq 100$ °C) with the corresponding set of temperature-dependent Pitzer coefficients is emphasized.

The presented thermodynamic model assumes the full dissociation of salts to Eu^{3+}, Mg^{2+}, Na^+ and NO_3^- ions. This drastically reduces the number of parameters, whose values however implicitly need to balance complexation effects expected in solution. Future work will incorporate spectroscopic data to target the description of complex formations in the ternary systems $Eu(NO_3)_3$-$NaNO_3$-H_2O and $Eu(NO_3)_3$-$Mg(NO_3)_2$-H_2O. A combination of the presented experimental results of this work and time resolved laser fluorescence spectroscopy

data enables the derivation of alternative SIT and Pitzer models, which consider the formation of aqueous complexes explicitly.

Conflicts of interest

There are no conflicts to declare.

Data availability

Additional data supporting this article have been included as part of the supplementary information (SI). Supplementary information: include additional XRD measurements, Rietveld refinement results, and the comparison of the full dissociation model results with osmotic coefficient data from literature. See DOI: https://doi.org/10.1039/d5ra09321j.

Acknowledgements

The present work was realized in the collaborative project co-funded by Andra, BRGM and KIT-INE.

References

1 J.-C. Bünzli, Europium in the Limelight, *Nat. Chem.*, 2010, **2**(8), 696, DOI: 10.1038/nchem.760.
2 N. Jordan, T. Thoenen, S. Starke, K. Spahiu and V. Brendler, A Critical Review of the Solution Chemistry, Solubility, and Thermodynamics of Europium: Recent Advances on the Eu^{3+} Aqua Ion and the Eu(III) Aqueous Complexes and Solid Phases with the Sulphate, Chloride, and Phosphate Inorganic Ligands, *Coord. Chem. Rev.*, 2022, **473**, 214608, DOI: 10.1016/j.ccr.2022.214608.
3 M. Altmaier, X. Gaona and T. Fanghänel, Recent Advances in Aqueous Actinide Chemistry and Thermodynamics, *Chem. Rev.*, 2013, **113**(2), 901–943, DOI: 10.1021/cr300379w.
4 V. Metz, W. Schüßler, B. Kienzler and T. Fanghänel, Geochemically Derived Non-Gaseous Radionuclide Source Term for the Asse Salt Mine – Assessment for the Use of a $Mg(OH)_2$-Based Backfill Material, *Radiochim. Acta*, 2004, **92**(9–11), 819–825, DOI: 10.1524/ract.92.9.819.54991.
5 B. A. Crawford, S. A. Lott, L. D. Sparks, G. Van Soest, and B. McInroy, The Road to Recertification: WIPP TRU Waste Inventory, in *Proceedings of Waste Management 2006 Conference*, WMS Tempe, AZ, 2006.
6 A. P. Paiva and P. Malik, Recent Advances on the Chemistry of Solvent Extraction Applied to the Reprocessing of Spent Nuclear Fuels and Radioactive Wastes, *J. Radioanal. Nucl. Chem.*, 2004, **261**(2), 485–496, DOI: 10.1023/B:JRNC.0000034890.23325.b5.
7 M. Herm, X. Gaona, T. Rabung, D. Fellhauer, C. Crepin, K. Dardenne, M. Altmaier and H. Geckeis, Solubility and Spectroscopic Study of AnIII/LnIII in Dilute to Concentrated Na–Mg–Ca–Cl–NO_3 Solutions, *Pure Appl. Chem.*, 2015, **87**(5), 487–502, DOI: 10.1515/pac-2014-1205.
8 H. Ma, M. Shen, Y. Tong and X. Wang, Radioactive Wastewater Treatment Technologies: A Review, *Molecules*, 2023, **28**(4), 1935, DOI: 10.3390/molecules28041935.
9 A. Lassin, P. F. dos Santos, X. Gaona, M. Altmaier, and B. Madé, Solution and Solid-Liquid-Equilibrium Properties of Radionuclide-Nitrate Aqueous Systems: Experiments and SIT Parameterization, in *Migration 2023*, Nantes, France, 2023.
10 L. Truche, G. Berger, A. Albrecht and L. Domergue, Abiotic Nitrate Reduction Induced by Carbon Steel and Hydrogen: Implications for Environmental Processes in Waste Repositories, *Appl. Geochem.*, 2013, **28**, 155–163, DOI: 10.1016/j.apgeochem.2012.10.010.
11 Y. Rafrafi, N. Durban, A. Bertron, A. Albrecht, J.-C. Robinet and B. Erable, Use of a Continuous-Flow Bioreactor to Evaluate Nitrate Reduction Rate of *Halomonas Desiderata* in Cementitious Environment Relevant to Nuclear Waste Deep Repository, *Biochem. Eng. J.*, 2017, **125**, 161–170, DOI: 10.1016/j.bej.2017.05.016.
12 Scandium, Yttrium, Lanthanum and Lanthanide Nitrates, 1, in *Solubility Data Series*, ed. S. Siekierski, T. Mioduski, and M. Salomon, Pergamon Press, Oxford New York Toronto Sydney Paris Frankfurt (Main) Kronberg-Taunus, 1983.
13 J. A. Rard, Solubility of $Eu(NO_3)_3 \cdot 6H_2O$ in Water at 298.15 K, *J. Chem. Thermodyn.*, 1984, **16**(10), 921–925, DOI: 10.1016/0021-9614(84)90159-9.
14 J. Eysseltová, V. Zbranek, M. Y. Skripkin, K. Sawada and S. Tepavitcharova, IUPAC-NIST Solubility Data Series. 89. Alkali Metal Nitrates. Part 2. Sodium Nitrate, *J. Phys. Chem. Ref. Data*, 2017, **46**(1), 013103, DOI: 10.1063/1.4972807.
15 L. Aït Hmaïdouch, S. Mançour Billah, M. El Hadek and G. Coffy, Etude Du Systeme Ternaire H_2O-$Al(NO_3)_3$-$Mg(NO_3)_2$ I - Isothermes 15, 25, 30, 40 et 50 °C, *J. Therm. Anal. Calorim.*, 2000, **61**(1), 165–171, DOI: 10.1023/A:1010177027734.
16 X. Yin, D. Li, Y. Tan, X. Wu, X. Yu and D. Zeng, Solubility Phase Diagram of the $Ca(NO_3)_2$–$Mg(NO_3)_2$–H_2O System, *J. Chem. Eng. Data*, 2014, **59**(12), 4026–4030, DOI: 10.1021/je500629s.
17 K. S. Pitzer, Thermodynamics of Electrolytes. I. Theoretical Basis and General Equations, *J. Phys. Chem.*, 1973, **77**(2), 268–277, DOI: 10.1021/j100621a026.
18 K. S. Pitzer, *Activity Coefficients in Electrolyte Solutions*, CRC Press, Boca Raton, FL, USA, 1991, vol. 2.
19 J. A. Rard, The Isopiestic Method: 100 Years Later and Still in Use, *J. Solution Chem.*, 2019, **48**(3), 271–282, DOI: 10.1007/s10953-019-00848-4.
20 J. A. Rard, and R. F. Platford, Experimental Methods: Isopiestic. Act. Coeff. Electrolyte Solut, in *Activity Coefficients in Electrolyte Solutions*, ed. K. S. Pitzer, CRC press Boca Raton, FL, 1991, vol. 2, pp. 209–277.
21 Y. Shahebrahimi and A. Fazlali, Vapor–Liquid Equilibrium of Aqueous Urea Solution from Dynamic Vapor Sorption Measurements at 283.15–343.15 K, *J. Chem. Eng. Data*, 2020, **65**(7), 3528–3535, DOI: 10.1021/acs.jced.9b01160.
22 Y. Cartigny and G. Coquerel, Impact of Solid/Vapour Equilibria on Conditions of Crystallization of Pharmaceutical Compounds, *Trans. Tianjin Univ.*, 2013, **19**(1), 53–57, DOI: 10.1007/s12209-013-1800-7.

23 T. Stumpf and M. Bolte, Tetra-aqua-trinitratoeuropium(III) Dihydrate, *Acta Crystallogr., Sect. E:Struct. Rep. Online*, 2001, **57**(2), i10–i11, DOI: 10.1107/S1600536801001271.

24 B. Ribár, A. Kapor, G. Argay and A. Kálmán, Tetraaquatrinitratoeuropium(III) Monohydrate, *Acta Crystallogr., Sect. C:Cryst. Struct. Commun.*, 1986, **42**(10), 1450–1452, DOI: 10.1107/S0108270186091928.

25 S. Göttlicher and C. D. Knöchel, Die Elektronendichteverteilung in Natriumnitrat (NaNO3), *Acta Crystallogr., Sect. B*, 1980, **36**(6), 1271–1277, DOI: 10.1107/S0567740880005900.

26 D. Baizar and H. Ledbetter, Accurate Modeling of Size and Strain Broadening in the Rietveld Refinement: The "Double-Voigt" Approach, *Adv. X-Ray Anal.*, 1994, **38**, 397–404, DOI: 10.1154/S0376030800018048.

27 F. A. H. Schreinemakers, Graphische Ableitungen aus den Lösungs-Isothermen eines Doppelsalzes und seiner Komponenten und mögliche Formen der Umwandlungskurve, *Z. Phys. Chem.*, 1893, **11U**(1), 75–109, DOI: 10.1515/zpch-1893-1107.

28 A. Dinane, Thermodynamic Properties of {NaCl-CsCl-LiCl}(aq) at T=298.15 K: Water Activities, Osmotic and Activity Coefficients, *J. Solution Chem.*, 2007, **36**(11), 1421–1436, DOI: 10.1007/s10953-007-9199-1.

29 J. C. Sohr, *Löslichkeitsgleichgewichte mit Lithiumsalzen und deren Modellierung mit dem Fokus auf das Salar-Brine-System bei tiefen Temperaturen*, TU Bergakademie Freiberg, Freiberg(Sachs), 2022.

30 C. E. Harvie and J. H. Weare, The Prediction of Mineral Solubilities in Natural Waters: The Na-K-Mg-Ca-Cl-SO_4-H_2O System from Zero to High Concentration at 25 °C, *Geochim. Cosmochim. Acta*, 1980, **44**(7), 981–997, DOI: 10.1016/0016-7037(80)90287-2.

31 G. Scatchard, Concentrated Solutions of Strong Electrolytes, *Chem. Rev.*, 1936, **19**(3), 309–327, DOI: 10.1021/cr60064a008.

32 L. André, A. Lassin, and A. Lach, *PHREESCALE.DAT: A Thermodynamic Database for the PhreeSCALE Software*, version 1.0, 2020, DOI: 10.18144/xy83-6848.

33 THEREDA - Thermodynamic Reference Database, 2024, https://www.thereda.de/.

34 P. F. dos Santos, A. Lassin, X. Gaona, K. Garbev, M. Altmaier and B. Madé, Thermodynamics of the Eu(III)–Mg–SO_4–H_2O and Eu(III)–Na–SO_4–H_2O Systems. Part I: Solubility Experiments and the Full Dissociation Pitzer Model, *Dalton Trans.*, 2024, **53**(14), 6289–6299, DOI: 10.1039/D3DT04322C.

35 C. Christov and N. Møller, Chemical Equilibrium Model of Solution Behavior and Solubility in the H-Na-K-OH-Cl-HSO_4-SO_4-H_2O System to High Concentration and Temperature, *Geochim. Cosmochim. Acta*, 2004, **68**(6), 1309–1331, DOI: 10.1016/j.gca.2003.08.017.

36 A. Lach, L. André and A. Lassin, Darapskite Solubility in Basic Solutions at 25 °C: A Pitzer Model for the Na-NO_3-SO_4-OH-H_2O System, *Appl. Geochem.*, 2017, **78**, 311–320, DOI: 10.1016/j.apgeochem.2016.12.008.

37 H. B. Silber, Europium(III) Complexation Reactions in Water, *Inorg. Chim. Acta*, 1987, **139**(1), 33–38, DOI: 10.1016/S0020-1693(00)84030-X.

38 L. Rao and G. Tian, Complexation of Lanthanides with Nitrate at Variable Temperatures: Thermodynamics and Coordination Modes, *Inorg. Chem.*, 2009, **48**(3), 964–970, DOI: 10.1021/ic801604f.

39 W. W. Rudolph, D. Fischer and G. Irmer, Hydration and Ion-Pair Formation of $NaNO_3$(aq): A Vibrational Spectroscopic and Density Functional Theory Study, *Appl. Spectrosc.*, 2021, **75**(4), 395–411.

40 B. Madé, W. Bower, S. Brassinnes, E. Colàs, L. Duro, P. Blanc, A. Lassin, L. Harvey and J. D. Begg, Recent Developments in ThermoChimie – A Thermodynamic Database Used in Radioactive Waste Management, *Appl. Geochem.*, 2025, **180**, 106273, DOI: 10.1016/j.apgeochem.2024.106273.

41 S. Guignot, A. Lassin, C. Christov, A. Lach, L. André and P. Henocq, Modeling the Osmotic and Activity Coefficients of Lanthanide Nitrate Aqueous Solutions at 298.15 K from Low Molalities to Supersaturation, *J. Chem. Eng. Data*, 2019, **64**(1), 345–359, DOI: 10.1021/acs.jced.8b00859.

42 A. Lach, L. André, S. Guignot, C. Christov, P. Henocq and A. Lassin, A Pitzer Parametrization To Predict Solution Properties and Salt Solubility in the H–Na–K–Ca–Mg–NO_3–H_2O System at 298.15 K, *J. Chem. Eng. Data*, 2018, **63**(3), 787–800, DOI: 10.1021/acs.jced.7b00953.

43 J. A. Rard and F. H. Spedding, Isopiestic Determination of the Activity Coefficients of Some Aqueous Rare-Earth Electrolyte Solutions at 25 °C. 6. Europium Trinitrate, Yttrium Nitrate, Yttrium Chloride, *J. Chem. Eng. Data*, 1982, **27**(4), 454–461, DOI: 10.1021/je00030a026.

44 P. R. Zalupski, R. McDowell and S. L. Clegg, Isopiestic Determination of the Osmotic Coefficients of $NaNO_3$ + $Eu(NO_3)_3$ + H_2O at 298.15 K and Representation with an Extended Ion-Interaction (Pitzer) Model, *J. Chem. Eng. Data*, 2014, **59**(5), 1574–1582, DOI: 10.1021/je500016d.

45 S. Chatterjee, E. L. Campbell, D. Neiner, N. K. Pence, T. A. Robinson and T. G. Levitskaia, Aqueous Binary Lanthanide(III) Nitrate $Ln(NO_3)_3$ Electrolytes Revisited: Extended Pitzer and Bromley Treatments, *J. Chem. Eng. Data*, 2015, **60**(10), 2974–2988, DOI: 10.1021/acs.jced.5b00392.

46 Y. C. Wu and W. J. Hamer, Revised Values of the Osmotic Coefficients and Mean Activity Coefficients of Sodium Nitrate in Water at 25 °C, *J. Phys. Chem. Ref. Data*, 1980, **9**(2), 513–518, DOI: 10.1063/1.555621.

47 M. El Guendouzi and M. Marouani, Water Activities and Osmotic and Activity Coefficients of Aqueous Solutions of Nitrates at 25 °C by the Hygrometric Method, *J. Solution Chem.*, 2003, **32**(6), 535–546, DOI: 10.1023/A:1025365900350.

48 R. A. Robinson, J. M. Wilson and H. S. Ayling, The Activity Coefficients of Some Bivalent Metal Nitrates in Aqueous Solution at 25° from Isopiestic Vapor Pressure Measurements, *J. Am. Chem. Soc.*, 1942, **64**(6), 1469–1471, DOI: 10.1021/ja01258a064.

49 J. A. Rard, A. M. Wijesinghe and T. J. Wolery, Review of the Thermodynamic Properties of $Mg(NO_3)_2$(aq) and Their Representation with the Standard and Extended Ion-Interaction (Pitzer) Models at 298.15 K, *J. Chem. Eng. Data*, 2004, **49**(5), 1127–1140, DOI: 10.1021/je049868l.

50 J. Doherty, *PEST Model-independent Parameter Estimation User Manual*, Watermark Numerical Computing, Brisbane, Australia, 2004, vol. 3338, p. 3349.
51 A. Lach, F. Boulahya, L. André, A. Lassin, M. Azaroual, J.-P. Serin and P. Cézac, Thermal and Volumetric Properties of Complex Aqueous Electrolyte Solutions Using the Pitzer Formalism – The PhreeSCALE Code, *Comput. Geosci.*, 2016, **92**, 58–69, DOI: 10.1016/j.cageo.2016.03.016.
52 C. Christov and N. A. Møller, Chemical Equilibrium Model of Solution Behavior and Solubility in the H-Na-K-Ca-OH-Cl-HSO_4-SO_4-H_2O System to High Concentration and Temperature, *Geochim. Cosmochim. Acta*, 2004, **68**(18), 3717–3739, DOI: 10.1016/j.gca.2004.03.006.
53 G. G. Urazov and Z. N. Shevtsova, *Russ. J. Inorg. Chem.*, 1957, **2**, 288–294, (data taken from: Scandium, Yttrium, Lanthanum and Lanthanide Nitrates, 1, ed. S. Siekierski, T. Mioduski, M. Salomon, Solubility Data Series; Pergamon Press, Oxford New York Toronto Sydney Paris Frankfurt (Main) Kronberg-Taunus, 1983).
54 E. F. Zhuravlev, Solubility in Ternary Aqueous Salt Systems Containing $Ce(NO_3)_3$ and an Alkali Metal Nitrate, *Russ. J. Inorg. Chem.*, 1963, **8**, 1017–1021.
55 M. A. Yakimov and E. I. Gizhavina, The $Ln(NO_3)_3$-$M(NO_3)_2$-H_2O Systems at 25 °C, *Russ. J. Inorg. Chem.*, 1971, **16**, 268–269, (data taken from: Scandium, Yttrium, Lanthanum and Lanthanide Nitrates, 1. ed. S. Siekierski, T. Mioduski, M. Salomon, Solubility Data Series, Pergamon Press, Oxford New York Toronto Sydney Paris Frankfurt (Main) Kronberg-Taunus, 1983).
56 N. V. Bunyakina, D. A. Storozhenko, V. G. Shevchuk and A. G. Dryuchko, Solubility Polytherm for the $Mg(NO_3)_2$-$Nd(NO_3)_3$-H_2O System, *Russ. J. Inorg. Chem.*, 1996, **41**(9), 1507–1509.
57 V. M. Akimov, A. I. Yanovskii, Y. T. Struchkov, A. K. Molodkin, Y. A. Grigor'ev and N. K. Novikov, The Crystal Structure of Magnesium Europium Nitrate-24-Water $Mg_3Eu_2(NO_3)_{12}(H_2O)_{24}$, *Zh. Neorg. Khim.*, 1987, **32**, 1547–1552.
58 Z.-P. Qiao, M.-Y. Su, Y.-L. Dang and Q.-C. Yang, Phase Equilibria in $Mg(NO_3)_2$–$Ln(NO_3)_3$ (Ln = Nd, Sm, Eu, Tb)–HNO_3 (~20%)–H_2O Systems at 298.15 K and Thermodynamic Properties of $Mg_3Ln_2(NO_3)_{12}\cdot 24H_2O$ (Ln = Nd, Sm), *J. Chem. Thermodyn.*, 2019, **136**, 116–122, DOI: 10.1016/j.jct.2019.05.001.
59 N. Jordan, T. Thoenen, K. Spahiu, J. Kelling, S. Starke and V. Brendler, A Critical Review of the Solution Chemistry, Solubility, and Thermodynamics of Europium: Recent Advances on the Eu(III) Hydrolysis, *Coord. Chem. Rev.*, 2024, **510**, 215702, DOI: 10.1016/j.ccr.2024.215702.
60 Y. V. Nelyubina, A. A. Korlyukov, K. A. Lyssenko and I. V. Fedyanin, Transferable Aspherical Atom Modeling of Electron Density in Highly Symmetric Crystals: A Case Study of Alkali-Metal Nitrates, *Inorg. Chem.*, 2017, **56**(8), 4688–4696, DOI: 10.1021/acs.inorgchem.7b00340.
61 J. Schefer and M. Grube, Low Temperature Structure of Magnesium Nitrate Hexahydrate, $Mg(NO_3)_2\cdot 6H_2O$: A Neutron Diffraction Study at 173 K, *Mater. Res. Bull.*, 1995, **30**(10), 1235–1241, DOI: 10.1016/0025-5408(95)00122-0.
62 A. Lassin, S. Guignot, A. Lach, C. Christov, L. André and B. Madé, Modeling the Solution Properties and Mineral–Solution Equilibria in Radionuclide-Bearing Aqueous Nitrate Systems: Application to Binary and Ternary Systems Containing U, Th, or Lanthanides at 25 °C, *J. Chem. Eng. Data*, 2020, **65**(7), 3613–3626, DOI: 10.1021/acs.jced.0c00180.
63 H. L. Silcock, Solubilities of Inorganic and Organic Compounds, *Ternary and Multicomponent Systems of Inorganic Substances*, Pergamon Press, 1979, vol. 3.
64 P. F. dos Santos, X. Gaona, A. Lassin, A. Skerencak-Frech, D. Fellhauer, M. Altmaier and B. Madé, Thermodynamics of the Eu(III)–Mg–SO_4–H_2O and Eu(III)–Na–SO_4–H_2O Systems. Part II: Spectroscopy Experiments, Complexation and Pitzer/SIT Models, *Dalton Trans.*, 2024, **53**(14), 6323–6332, DOI: 10.1039/D3DT04323A.